Walén and slow-mode shock analyses in the near-Earth magnetotail in connection with a substorm onset on 27 August 2001

S. Eriksson,[1] M. Øieroset,[2] D. N. Baker,[1] C. Mouikis,[3] A. Vaivads,[4] M. W. Dunlop,[5] H. Rème,[6] R. E. Ergun,[1] and A. Balogh[7]

Received 9 April 2004; revised 16 July 2004; accepted 6 August 2004; published 23 October 2004.

[1] We have examined Cluster spacecraft 1 (C1) magnetic field and particle observations from 27 August 2001 when the Cluster spacecraft separation was less than 0.27 R_E and the spacecraft were located near the equatorial plane of the postmidnight magnetotail at $x_{GSM} \sim -19\ R_E$ and $y_{GSM} \sim -2.1\ R_E$. A detailed examination of observations recorded between 0350 UT and 0435 UT is performed with special emphasis on the plasma flow reversal from strong tailward flows to earthward flows in the approximate time interval 0400 UT to 0410 UT. Evidence for the expansion phase onset of an isolated substorm between ~0406 UT and ~0408 UT was reported by *Baker et al.* [2002]. During the 0400–0410 UT interval, C1 was located in the plasma sheet where the observed plasma density $N \sim 0.3$ cm^{-3} and the plasma ion $\beta \sim 1.5$. The Walén analysis applied to the tailward flow interval from 0400:36 UT to 0403:14 UT is consistent with the ions being accelerated to ~73% of the Alfvén speed across a slow-mode shock connected to a near-Earth neutral line located on the earthward side of the spacecraft. The occurrence of a small plasmoid-type magnetic flux rope during the leading edge of the tailward flows provides further support in favor of an active region of magnetic reconnection earthward of Cluster. The more field-aligned earthward flows between 0406 UT and 0408 UT, however, failed to satisfy the Walén test. Rankine-Hugoniot analyses of upstream and downstream plasma and magnetic field parameters confirm the presence of a slow-mode shock in connection with the passage of the tailward flow region but not with the 0406 UT to 0408 UT earthward flow interval. The confirmed shock satisfies the critical slow-mode requirements: $M_I^* \leq 1.0$ and $M_{SM}^* > 1.0$ on the upstream side and $M_{SM}^* < 1.0$ on the downstream side. Here, M_I^* and M_{SM}^* are the intermediate Alfvén speed and slow-mode phase speed Mach numbers in the frame of the shock. The failure of both the Walén test and the Rankine-Hugoniot analysis on the earthward flow portion of the plasma reversal event may be associated with the strong earthward $\nabla\mathbf{B}$ of the inner magnetosphere. The successful joint Walén and slow shock analyses on the tailward flows within the plasma sheet present further evidence in favor of Petschek-type reconnection at distances $x_{GSM} > -19\ R_E$ of the near-Earth magnetotail. *INDEX TERMS:* 7835 Space Plasma Physics: Magnetic reconnection; 7851 Space Plasma Physics: Shock waves; 2744 Magnetospheric Physics: Magnetotail; 2788 Magnetospheric Physics: Storms and substorms; *KEYWORDS:* magnetic reconnection, shock waves, magnetotail boundary layers

Citation: Eriksson, S., M. Øieroset, D. N. Baker, C. Mouikis, A. Vaivads, M. W. Dunlop, H. Rème, R. E. Ergun, and A. Balogh (2004), Walén and slow-mode shock analyses in the near-Earth magnetotail in connection with a substorm onset on 27 August 2001, *J. Geophys. Res.*, *109*, A10212, doi:10.1029/2004JA010534.

[1]Laboratory for Atmospheric and Space Physics, University of Colorado, Boulder, Colorado, USA.
[2]Space Sciences Laboratory, University of California, Berkeley, California, USA.
[3]Space Science Center, University of New Hampshire, Durham, New Hampshire, USA.
[4]Swedish Institute of Space Physics, Uppsala, Sweden.
[5]Rutherford Appleton Laboratory, Chilton, UK.
[6]Centre d'Etude Spatiale des Rayonnements, Toulouse, France.
[7]The Blackett Laboratory, Imperial College, London, UK.

0148-0227/04/2004JA010534$09.00

1. Introduction

[2] Magnetic reconnection in the neutral sheet of the magnetotail is often cited as a major mechanism in the generation of substorms and fast plasma flows in the tail [e.g., *Hones et al.*, 1986; *Angelopoulos et al.*, 1992; *Baker et al.*, 1996]. Tail reconnection is also considered to be an integral part of the global plasma convection in the magnetosphere and provides a driving mechanism for the earthward return flow of magnetic flux [e.g., *Dungey*, 1961].

[3] *Øieroset et al.* [2000] presented Wind observations from an encounter with high-speed flows lasting several hours in the midtail region at $x \sim -60\ R_E$. They applied the shear stress balance test which is often referred to as the Walén test [e.g., *Walén*, 1944; *Sonnerup et al.*, 1987] to the fast flows and showed that the field-aligned flow speeds in the deHoffmann-Teller (HT) frame [*deHoffmann and Teller*, 1950; *Khrabrov and Sonnerup*, 1998] averaged ~60% of the Alfvén speed and never exceeded the Alfvén speed. Sub-Alfvénic speeds are consistent with the presence of slow-mode shocks connected to the diffusion region [*Petschek*, 1964] that would generally limit the expected acceleration of the ions across the shock layer to sub-Alfvénic velocities [*Hau and Sonnerup*, 1989].

[4] Slow-mode shocks were first observed in the distant magnetotail based on ISEE-3 measurements [*Feldman et al.*, 1984; *Smith et al.*, 1984] using the Rankine-Hugoniot shock jump conditions and subsequently also reported in the near-Earth tail [*Feldman et al.*, 1987] in conjunction with a well-examined substorm event [*Hones et al.*, 1986]. In traversing a slow shock, the plasma pressure is predicted to increase while the magnetic pressure should decrease from the upstream side to the downstream side of the shock [e.g., *Saito et al.*, 1995; *Seon et al.*, 1996]. It is therefore expected that the entropy of the ions and electrons should increase as the shock is traversed due to the irreversible dissipation processes in the shock layer.

[5] Observational evidence for reconnection in terms of the Hall effect has recently been reported in the near-Earth tail [*Nagai et al.*, 2001, 2003; *Runov et al.*, 2003] as well as in the midtail region [e.g., *Deng et al.*, 2004]. These studies confirm the expected Hall current effects and quadrupolar magnetic field signatures in the $\pm B_y$ direction in the vicinity of a neutral line [*Sonnerup*, 1979].

[6] In the present study we report quantitative evidence for magnetic reconnection during a tailward jet interval observed by Cluster in the plasma sheet of the near-Earth magnetotail. We perform both the Walén test (section 3) and the Rankine-Hugoniot (RH) shock jump condition analysis (section 4) to test whether the observed jets were accelerated across Petschek-type slow-mode shocks. An examination of the applied shock normal directions which are of critical importance to the RH analyses appears in section 4.2. The results from this event study are discussed in section 5, followed by a summary and conclusions in section 6.

2. Cluster Observations

[7] A comprehensive overview of this event in terms of substorm dynamics was presented by *Baker et al.* [2002]. We here focus on the aspect of showing quantitatively that the accelerated flows observed by Cluster in the near-Earth magnetotail were indeed consistent with magnetic reconnection.

[8] The four Cluster spacecraft [*Escoubet et al.*, 2001] have an identical set of instruments to measure the magnetic field and the plasma parameters. The Fluxgate Magnetometer (FGM) experiment [*Balogh et al.*, 2001] consists of two triaxial fluxgate magnetic field sensors. The Cluster Ion Spectrometry (CIS) experiment [*Rème et al.*, 2001] measures full three-dimensional ion distributions of major magnetospheric species such as H^+ and O^+ from thermal energies to ~40 keV/e. The CIS instrument comprises two separate instruments: the "top hat" electrostatic Hot Ion Analyser (HIA) sensor, with a 5.6° angular resolution, and the time-of-flight mass-resolving ion Composition and Distribution Function (CODIF) spectrometer. The energy range of the HIA sensor is approximately 5 eV/e to 32 keV/e, while the energy range of the CODIF instrument (22.5° angular resolution) is ~20 eV/e to 38 keV/e. This study applies FGM magnetic field data and CIS plasma data at 4-s spin resolution. The GSM coordinate system is applied throughout.

[9] An overview of the Cluster spacecraft 1 (C1) spin resolution plasma and magnetic field data recorded between 0350 UT and 0435 UT on 27 August 2001 is displayed in Figure 1. The panels from the top show the total plasma density using H^+ and O^+ measurements from the CODIF instrument, the derived ion β (CODIF data), the magnitude of the ion velocity (HIA instrument data), the three GSM components of the ion velocity (x is black, y is green, and z is red), the angle between the velocity and magnetic field where 90° corresponds to a purely convective velocity component, the three GSM components of the magnetic field (same color code as the velocity), and the total magnetic field $|\mathbf{B}|$. The GSM location of Cluster C1 is found along the time axis below the panels in Figure 1.

[10] Measurements from Cluster spacecraft 3 (C3) and spacecraft 4 (C4) display very similar signatures in both the magnetic field and the plasma velocity as C1 during this time period [see *Baker et al.*, 2002, Figure 4]. The separation between C1 and C3 ranges between ~909 km and ~1393 km, while the separation between C1 and C4 was found between ~472 km and ~1720 km. We will therefore concentrate our Walén and shock jump analyses on observations from C1. Data from the CODIF sensor are employed for all plasma quantities except for the bulk velocity where HIA data were utilized. The bulk velocity from HIA and CODIF are nearly identical.

[11] Several periods of fast ion flows are observed in Figure 1 that reach magnitudes of 400 km/s or more. Three such intervals are indicated in between or near the vertical dash-dot lines in Figure 1 which mark the selected time periods for the Walén analysis in section 3. The onset of a tailward flow region is observed by Cluster C1 at 0401:18 UT. The mostly convective tailward flows then reverse direction and become earthward at 0406:00 UT. The earthward flows are more field-aligned than the tailward flows with an angle between $\mathbf{V}$ and $\mathbf{B}$ that approximately ranges between 30° and 50° (see third panel from the bottom).

[12] The magnetic field further suggests the presence of a ~45 s long magnetic flux rope [e.g., *Slavin et al.*, 2003b] during the leading edge of the tailward flow region. The small flux rope is centered near 0401:52 UT (dotted vertical line) with a positive $B_z = 4.0$ nT perturbation at 0401:47 UT followed by a negative $B_z = -3.4$ nT deflection at 0402:03 UT. The dawnward ($B_y < 0$) increase in the B_y component at 0401:52 UT produces a peak in $|\mathbf{B}|$ suggesting that the flux rope may be force-free [*Slavin et al.*, 2003b].

[13] The average plasma β and total density during these intervals of tailward flow ($\beta = 1.54$ and $N = 0.31\ \mathrm{cm}^{-3}$) and earthward flow ($\beta = 0.55$ and $N = 0.12\ \mathrm{cm}^{-3}$) marked

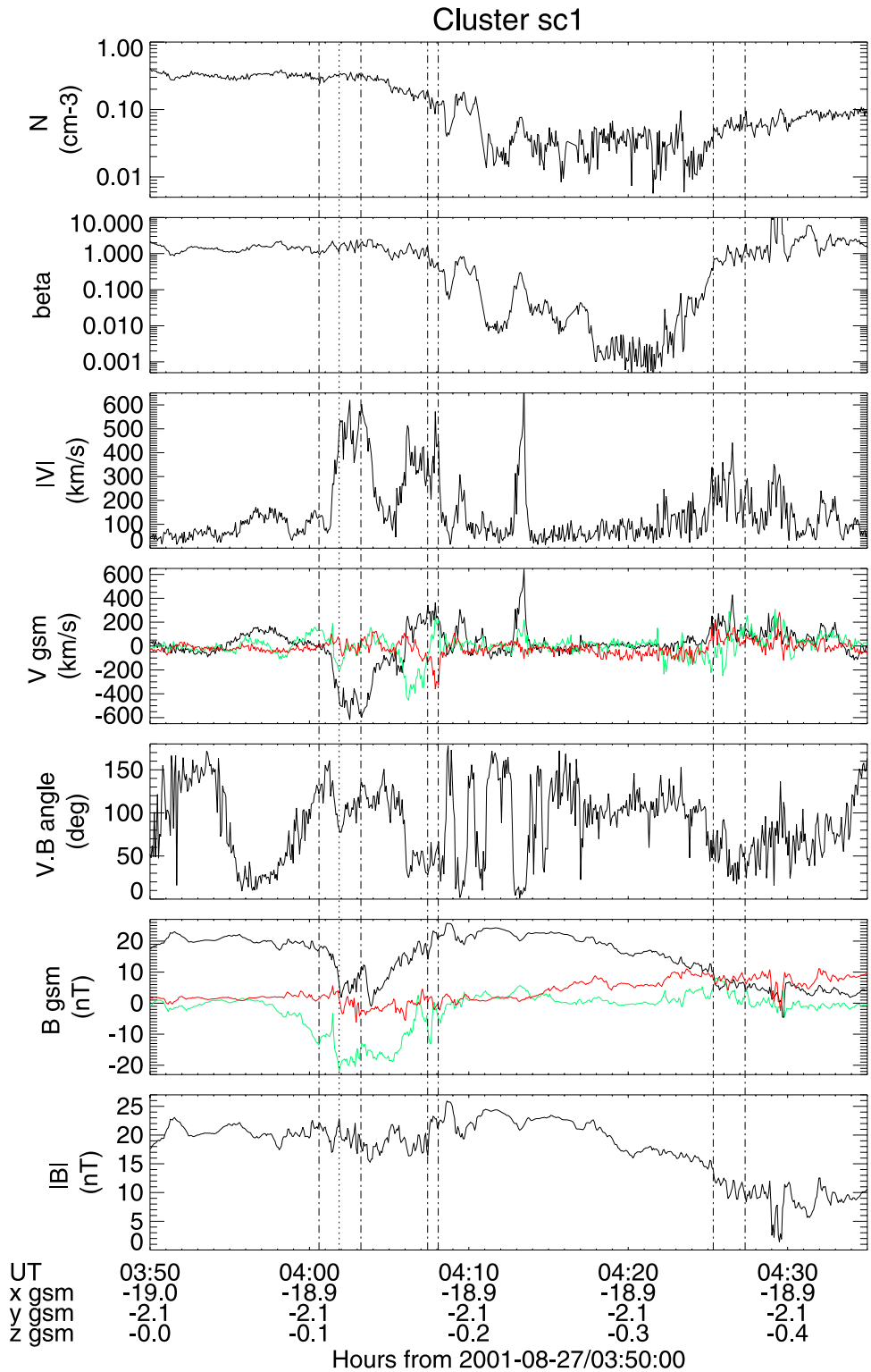

Figure 1. An overview of Cluster C1 plasma and magnetic field data recorded between 0350 UT and 0435 UT on 27 August 2001. The panels from the top show the total plasma density and the ion plasma β based on H^+ and O^+, the magnitude of the ion velocity, the three GSM components of the ion velocity, the angle between the velocity and the magnetic field, the three GSM components of the magnetic field, and the total magnetic field. The GSM components are color coded with *x* in black, *y* in green, and *z* in red. The dotted line mark the center of a plasmoid-type magnetic flux rope, while the dashed-dotted lines separate the time intervals for the Walén analyses.

between the dashed vertical lines in Figure 1 are characteristic of the plasma sheet proper [*Baumjohann et al.*, 1990]. The observed flow reversal also coincides with a rotation of the magnetic field (second panel from the bottom) from a predominant earthward direction prior to the fast tailward flows to a mostly dawnward direction during the tailward flow region, suggesting the downtail release of a plasmoid [see *Slavin et al.*, 2003a, and references therein]. The field then returns to an earthward direction as the flow also turns earthward. A temporary southward excursion of the magnetic field was also detected during the trailing part of the tailward flow region with a minimum near $B_z = -6$ nT.

[14] The plasma sheet interval is followed by a prolonged period of low density and low ion plasma β after 0410:24 UT while the B_x component stayed positive, suggesting that the northern tail lobe region encompassed Cluster until ~0422 UT when the plasma sheet began to recover over the spacecraft. This recovery occurred as $|\mathbf{B}|$ was decreasing, while the positive B_z component steadily increased and the positive B_x component gradually decreased. Enhanced earthward flows were also being observed as the ion plasma β recovered to its plasma sheet levels.

[15] Global auroral UV images from IMAGE and GOES-8 signatures of field dipolarization and current disruption [*Baker et al.*, 2002] set an approximate substorm onset within the 0406 UT to 0408 UT interval when earthward flows were detected at Cluster. This time period followed the observed tailward flow onset at ~0401 UT by 5 min or more, suggesting that reconnection developed at a near-Earth neutral line prior to current disruption and dipolarization.

3. Walén Analyses

[16] Whether the enhanced ion speeds observed by Cluster in the near-Earth tail on 27 August 2001 are in agreement with acceleration due to reconnection or not may be examined by applying the shear stress balance test (also known as the Walén test) to the measured ion velocity and the magnetic field in the proximity of the assumed one-dimensional and time-independent slow shock boundary. Ideal MHD predicts that the magnetic field and plasma velocity across a rotational discontinuity at the magnetopause may be stated as

$$\mathbf{V} - \mathbf{V}_{HT} = \pm \frac{\mathbf{B}\sqrt{(1-\alpha)}}{\sqrt{\rho_f \mu_0}} \quad (1)$$

in the deHoffmann-Teller (HT) frame of reference [*Sonnerup et al.*, 1987], where $\mathbf{V}$ is the plasma velocity, $\mathbf{V}_{HT}$ is the HT frame velocity, $\mathbf{B}$ is the magnetic field, and α is the pressure anisotropy factor defined as $(p_{\|} - p_{\perp})\,\mu_0/B^2$. The plasma pressures parallel and perpendicular to $\mathbf{B}$ are denoted by $p_{\|}$ and $p_{\perp}$, respectively. The effective mass density $\rho_f = Nm_f$ assumes an effective mass $m_f = \Sigma_i n_i m_i / N$ that ideally incorporates the mass m_i of all ion species where N is the total plasma density. The above Walén relation thus predicts that the plasma velocity $\mathbf{V}' = \mathbf{V} - \mathbf{V}_{HT}$ in the HT frame is field-aligned and that it should correspond to the Alfvén velocity for reconnection events at the magnetopause [e.g., *Phan et al.*, 2001].

[17] However, as shown by *Hau and Sonnerup* [1989] and *Øieroset et al.* [2000], it is expected that the shear stress balance relation in equation (1), which is valid for rotational discontinuities at the magnetopause, has to be modified by the strength of the local slow-mode shock assumed to be connected to the reconnection regions of the magnetotail. The modification is determined by the range of locally observed Alfvén Mach numbers M_A^* upstream and downstream of the shock and results in constants of proportonality that are generally lower than one for slow-mode shocks. The modified Walén relation for the case of an approximately isotropic plasma pressure becomes

$$\mathbf{V} - \mathbf{V}_{HT} = \pm M_A^* \frac{\mathbf{B}}{\sqrt{\rho_f \mu_0}}, \quad (2)$$

where $M_A^* = \tilde{V}_n / V_A$ and $\tilde{V}_n$ is the component of the plasma velocity normal to the shock boundary evaluated in the frame of the shock [*Seon et al.*, 1996]. The Alfvén speed is given as $V_A = |\mathbf{B}|/\sqrt{\rho_f \mu_0}$. It is therefore expected that the value of the regression slope should reflect the range of M_A^* if equation (1) is applied to accelerated flows in the vicinity of magnetotail slow-mode shocks.

[18] The sign of the regression slope from equation (1) in a scatter plot of the components of $\mathbf{V}'$ versus the Alfvén velocity depends on whether the field-aligned velocity $\mathbf{V}'$ in the HT frame is parallel or antiparallel to the magnetic field across the slow shock. The Walén slope is therefore predicted to be positive (negative) for tailward jets on the northern (southern) side of the neutral sheet as well as for earthward jets on the southern (northern) side of the neutral sheet [see also *Øieroset et al.*, 2000].

[19] The three time intervals of enhanced plasma flows indicated in Figure 1 were eventually selected for detailed Walén analyses using equation (1). All three jet intervals were observed north of the neutral sheet as determined by the positive B_x components of the magnetic field. The left-hand column of Figure 2 displays the components of the field-aligned ion velocity $\mathbf{V}'$ in the HT frame versus the estimated Alfvén velocity. It is assumed that the plasma consists of H^+ and O^+ alone, thus yielding an effective mass density m_f from the CODIF ion composition instrument. Second, we assume that the plasma pressure is approximately isotropic. The x, y, and z components of the displayed vectors on the vertical and horizontal axes are color coded in blue, green, and red, respectively. The HT frame for the chosen time intervals was retrieved following the procedure described by *Sonnerup et al.* [1987].

[20] The quality of the individually deduced HT frames is illustrated in the right-hand column of Figure 2, where the measured convective electric field is compared with the estimated electric field using the HT velocity. Since the HT frame is defined as that frame where the convective electric field ideally vanishes, it is expected for $(\mathbf{V} - \mathbf{V}_{HT}) \times \mathbf{B}$ to be nearly zero for a high-quality HT frame which corresponds to the observed data being located along the diagonals in the right-hand column of Figure 2. Note that the axis range varies in Figures 2a–2c such that a direct intercomparison between the quality of the HT frames in the different intervals could be misleading. Good HT frames were found for the intervals in Figure 2a and Figure 2c but not for the interval in Figure 2b where the slope is slightly off-diagonal.

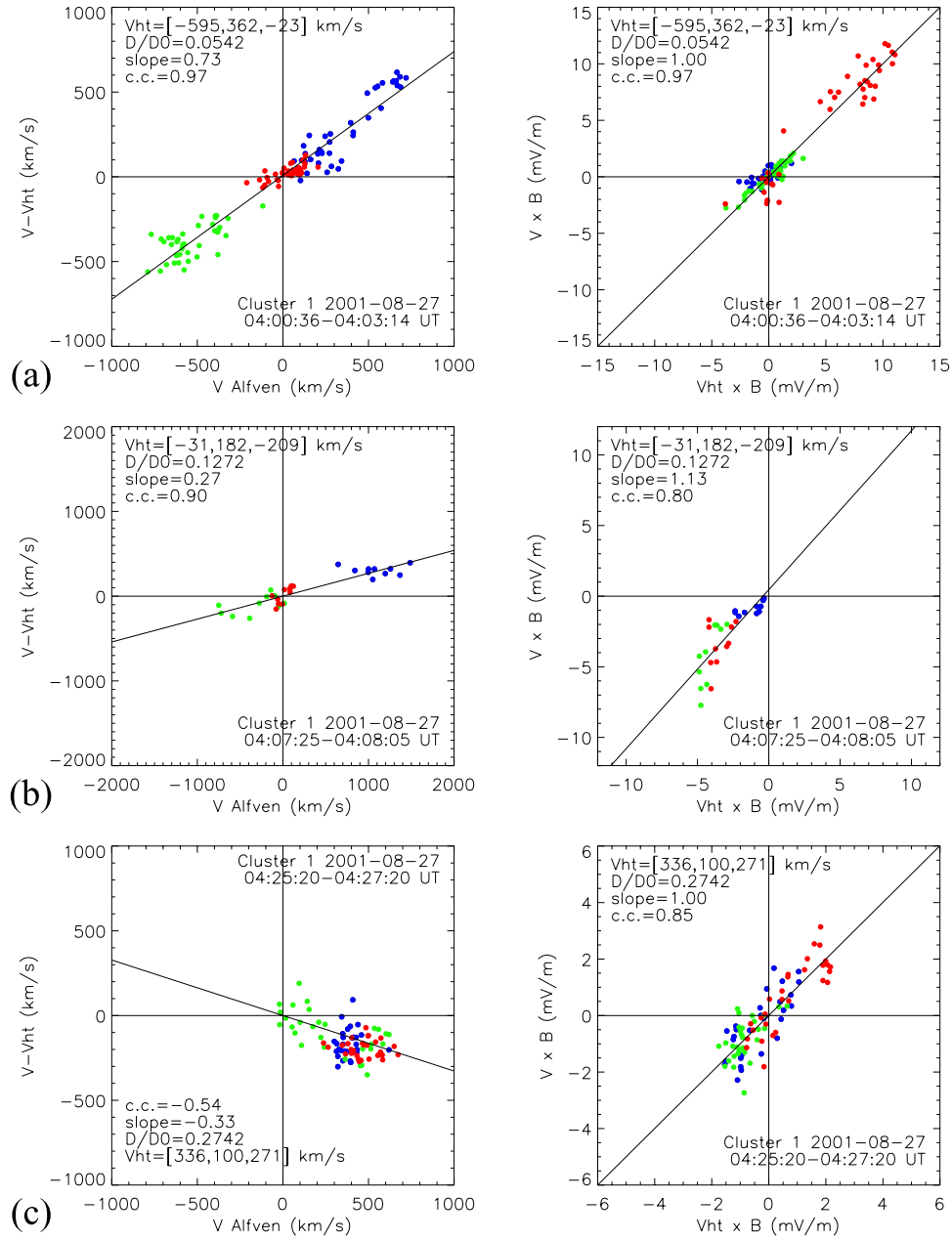

Figure 2. Walén analyses for three time periods (a–c) as displayed between the vertical lines in Figure 1. The field-aligned flow velocity in the HT frame is shown versus the Alfvén velocity in the left-hand column. The x_{GSM}, y_{GSM}, and z_{GSM} components are shown as blue, green, and red dots, respectively. The correlation coefficient, the best fit regression slope, the quality ratio of the HT frame D/D_0, and the HT velocity are all shown explicitly for each time period. The right-hand column indicate the quality of the HT frame where the measured data should fall on the diagonal for a good HT frame.

[21] The Walén analysis applied to the Cluster C1 data between 0400:36 UT and 0403:14 UT (Figure 2a) indicates that the measured $\mathbf{V}'$ equals 73% of the Alfvén velocity (the obtained regression slope) for the tailward flow interval in this high-quality HT frame. The Walén slope is positive, which is in agreement with Cluster observing tailward plasma jets on the northern side of the neutral sheet under the assumption that a near-Earth neutral line exists earthward of Cluster and that the plasma is accelerated across a Petschek-type slow-mode shock connected to the diffusion region.

[22] When equation (1) is applied to the time interval from 0407:25 UT to 0408:05 UT (Figure 2b) or any other time period during the earthward flow immediately following the tailward flows, it is found that the Walén test results in regression slopes of poor quality. This suggests that the observed plasma and magnetic fields could not be interpreted in terms of a quasi-steady and well-organized, one-dimensional boundary such as a slow-mode shock. The indicated positive regression slope is, furthermore, in contrast to the expected negative slopes during these conditions of observed earthward

flows in the northern ($B_x > 0$) magnetotail region [*Øieroset et al.*, 2000].

[23] We also applied the Walén test to the 0425:20 UT to 0427:20 UT interval during the plasma sheet recovery when earthward flows were being observed in the northern magnetotail (see Figure 1). The result is shown in Figure 2c. The comparison of the convective electric fields (right-hand side) indicate a rather well-determined HT frame of reference. Although the Walén slope is of questionable quality (correlation coefficient of −0.54), it appears that the Walén relation results in a negative slope at 33% of the Alfvén velocity. A negative slope is also to be expected for ions being accelerated in the earthward direction on the northern side of the neutral sheet upon traversing a slow-mode shock assumed to be connected to a neutral line located tailward of Cluster [see *Øieroset et al.*, 2000].

[24] In summary, the Walén test was satisfied for the tailward flow portion of the event, with an excellent correlation coefficient of 0.97 and a positive slope of 0.73, consistent with the spacecraft being tailward of the neutral line in the Northern Hemisphere. The Walén test was not satisfied for the earthward flows immediately following the tailward flows, although the negative slope obtained for the recovery flows almost 20 min after the flow reversal is consistent with a location of the spacecraft earthward of a neutral line in the Northern Hemisphere.

4. Slow-Mode Shock Analyses

[25] Whether the plasma was accelerated across a shock or not may be examined by studying the Rankine-Hugoniot (RH) shock jump conditions and by verification that the entropy indeed increases over the chosen interval. On the basis of the Sackur-Tetrode equation for a monatomic gas, the total entropy S for the protons may be expressed as

$$S = k_B\left(\frac{3}{2}\ln\left(2\pi m_p k_B T/h^2\right) - \ln(n) + \frac{5}{2}\right), \tag{3}$$

where T is the proton temperature (in °K), n is the proton density, m_p is the proton mass, k_B is the Boltzmann constant, and h is the Planck constant. This gives an expression for the change in total entropy $\Delta S = S_d - S_u$ [see also *Smith et al.*, 1984] between the downstream and the upstream sides of the shock as $\Delta S/k_B = \frac{3}{2}\ln(T_d/T_u) - \ln(n_d/n_u)$. Subscripts d and u denotes the downstream and upstream sides of the shock, respectively.

[26] The jump in any quantity X on either side of a shock boundary may be expressed as $[X] = X_u - X_d$. Using this notation and based on the MHD conservation equations, the complete set of RH shock jump conservation relations [*Burgess*, 1995, and references therein] are stated as

$$\left[\rho_f \tilde{V}_n\right] = 0 \tag{4}$$

$$\left[\rho_f \tilde{V}_n^2 + P_p + \frac{B^2}{2\mu_0}\right] = 0 \tag{5}$$

$$\left[\rho_f \tilde{V}_n\left(\frac{\tilde{V}^2}{2} + \frac{\gamma}{\gamma-1}\frac{P_p}{\rho_f} + \frac{B^2}{\mu_0\rho_f}\right) - \frac{B_n\tilde{\mathbf{V}}\cdot\mathbf{B}}{\mu_0}\right] = 0 \tag{6}$$

$$[B_n] = 0 \tag{7}$$

$$\left[\rho_f \tilde{V}_n\tilde{\mathbf{V}}_t - \frac{B_n\mathbf{B}_t}{\mu_0}\right] = 0 \tag{8}$$

$$\left[B_n\tilde{\mathbf{V}}_t - \tilde{V}_n\mathbf{B}_t\right] = 0, \tag{9}$$

where the total plasma bulk velocity $\tilde{\mathbf{V}}$ in the rest frame of the shock boundary is related to the measured GSM velocity $\mathbf{V}$ as $\tilde{\mathbf{V}} = \mathbf{V} - \mathbf{V}_{sh}$ and $\mathbf{V}_{sh}$ is the estimated shock velocity. P_p is the total kinetic plasma pressure and γ is the ratio of specific heats at constant volume and constant pressure. It is assumed that $\gamma = 5/3$. The normal and tangential components of the velocity and the magnetic field in the shock frame of reference are denoted by subscripts n and t, respectively.

[27] Equations (4) through (9) correspond to the conservation of mass, normal momentum, energy flow, normal magnetic field, transverse momentum, and the continuity of the tangential electric field, respectively. Note that we assume no additional heat flux in equation (6) and that equation (9) assumes a quasi-steady magnetic field $\partial\mathbf{B}/\partial t = 0$.

[28] The normal component of the shock velocity $\mathbf{V}_{sh}$ is found by solving equation (4) based on the relation $\tilde{\mathbf{V}} = \mathbf{V} - \mathbf{V}_{sh}$ as

$$\mathbf{V}_{sh}\cdot\hat{\mathbf{n}} = \frac{\rho_d\mathbf{V}_d\cdot\hat{\mathbf{n}} - \rho_u\mathbf{V}_u\cdot\hat{\mathbf{n}}}{\rho_d - \rho_u}, \tag{10}$$

where subscripts d and u denote the selected downstream and upstream intervals on either side of the shock boundary. Here, it is assumed that the shock velocity $\mathbf{V}_{sh}$ is aligned with the shock boundary normal $\hat{\mathbf{n}}$.

[29] We initially estimate a shock normal direction by using the magnetic coplanarity theorem, which states that the upstream and downstream magnetic fields are in the same plane as the shock normal. This gives the following expression for the shock normal

$$\hat{\mathbf{n}} = \pm\frac{(\mathbf{B}_u\times\mathbf{B}_d)\times(\mathbf{B}_u - \mathbf{B}_d)}{|(\mathbf{B}_u\times\mathbf{B}_d)\times(\mathbf{B}_u - \mathbf{B}_d)|}. \tag{11}$$

The set of RH conditions may now be examined to determine whether a shock layer is present in between any selected pairs of upstream and downstream time intervals by using equations (10) and (11). The validity of the magnetic coplanarity shock normal based on the plasma and magnetic field measurements from Cluster C1 is further analyzed in section 4.2.

[30] There are, moreover, a set of requirements to be satisfied for a slow-mode type of shock. We utilize the following initial set of slow-mode shock conditions: (1) the plasma pressure P_p increases across the boundary, (2) the magnetic pressure P_b decreases across the boundary, and (3) the propagation angle θ_B of the direction of the wave decreases across the boundary (i.e., the magnetic field bends toward the boundary normal direction). The angle θ_B is retrieved as $\theta_B = \arccos(\mathbf{B}\cdot\hat{\mathbf{n}}/|\mathbf{B}|)$.

[31] Another set of critical requirements for the confirmation of slow-mode shocks [e.g., *Omidi and Winske*, 1989;

Seon et al., 1996] is that (1) the upstream intermediate Alfvén Mach number $M_I^* \leq 1.0$, (2) the upstream slow-mode magnetosonic Mach number $M_{SM}^* > 1.0$, and (3) the downstream slow-mode magnetosonic Mach number $M_{SM}^* < 1.0$. Here, $M_I^* = \tilde{V}_n/V_I$ and $M_{SM}^* = \tilde{V}_n/V_{SM}$, where the intermediate mode Alfvén speed V_I, the sound speed V_S, and the slow-mode magnetosonic phase speed V_{SM} are given as follows:

$$V_I = V_A \cos\theta_B \tag{12}$$

$$V_S = \sqrt{\frac{\gamma P_p}{\rho_f}} \tag{13}$$

$$V_{SM} = \sqrt{\frac{\left(V_S^2 + V_A^2\right) - \sqrt{\left(V_S^2 + V_A^2\right)^2 - 4V_S^2 V_I^2}}{2}}. \tag{14}$$

4.1. Application of the Rankine-Hugoniot Relations

[32] In order to compare the results from the Walén analyses with the assumption that slow-mode shocks accelerated the plasma observed at Cluster, we now apply the given RH requirements and slow-mode shock criteria for three sets of upstream and downstream time intervals. The selected times for the downstream periods should be located in relative proximity to the observed plasma speed enhancements marked within the vertical lines in Figure 1. A clear increase in the H^+ temperature is also utilized in the selection of the downstream time period. The upstream intervals will be found at some time prior to the downstream events or before the arrival at Cluster of the assumed shocks which stand in the flow. The upstream regions thus ought to reflect an average plasma sheet bulk speed on the order of 150 km/s or lower (see Figure 1) with a proton temperature that is clearly lower than downstream.

[33] Figure 3 displays a number of plasma and magnetic field quantities relevant to the shock analysis. From the top, these are the total H^+ and O^+ plasma density N, the ion plasma β, the H^+ temperature, the total H^+ entropy from equation (3), the total plasma and magnetic field pressure, the kinetic plasma pressure P_p, the plasma bulk speed, and the magnetic field magnitude $|\mathbf{B}|$. The selected three pairs of upstream and downstream time intervals are indicated by vertical bars in the bottom panel. As seen in the total magnetic field, there is a tendency toward higher $|\mathbf{B}|$ during the indicated upstream intervals as compared with the downstream periods which is expected for slow-mode shocks. The H^+ temperatures are also higher downstream than upstream, which is generally reflected in the total kinetic plasma pressure as well.

[34] The magnetic coplanarity theorem in equation (11) is first applied to retrieve the estimated boundary normals for the average magnetic fields during the separate upstream and downstream intervals. We then derive the shock velocity using equation (10) and find the H^+ entropy change from equation (3) by use of the average ion bulk velocity $\mathbf{V}$ and H^+ temperature and density. The resulting boundary normals $\hat{\mathbf{n}}$ and shock velocities $\mathbf{V}_{sh}$ (in GSM) are listed in Table 1 together with the entropy changes ΔS (in meV/K) for their respective upstream and downstream time intervals. The resulting ΔS indicate that the entropy generally increases across all three boundaries, since this quantity is positive that supports the presence of shocks.

[35] The derived shock normals and shock velocities in Table 1 are now used to verify whether or not the three boundaries can be identified as shocks and in particular whether the slow-mode shock criteria stated previously are satisfied across the boundaries. The complete shock analysis using the averaged quantities during the three upstream and downstream intervals in Figure 3 is found in Table 2. Note that the RH jump condition for the conservation of mass (RH_1) and the jump condition for the normal magnetic field (RH_4) are satisfied by definition for all boundaries, since these were used to derive the shock velocity and normal.

[36] The observed upstream normal momentum (RH_2) and the upstream energy flow (RH_3) for the first boundary near the tailward flow region are observed within 3% and 8% of the downstream momentum and energy flow quantities, respectively. The average tangential momentum (RH_5) and the tangential electric field (RH_6) are also found within 10% and 29% of the downstream levels, respectively. These deviations should be compared with the 30% energy criterion used by *Saito et al.* [1995] as a shock indicator. It is therefore quite likely that the nature of this first boundary satisfies that of a shock based on the applied RH jump conditions and the increase in entropy.

[37] Concerning the characterization of the first shock, we further observe that (1) $P_p^d > P_p^u$ by ~22%, (2) $P_b^d < P_b^u$ by ~19%, and (3) $\theta_B^d < \theta_B^u$. This indicates a slow-mode character of the shock. However, these measurements also suggest that (1) $M_I^* = 0.86$ on the upstream side, (2) $M_{SM}^* = 1.07$ on the upstream side, and (3) $M_{SM}^* = 0.85$ on the downstream side of the shock. These Mach number conditions thus satisfy the more stringent criteria for a slow-mode shock in the vicinity of the tailward flow region as suggested by, e.g., *Seon et al.* [1996], and we conclude that a slow-mode shock most likely passed Cluster C1 in between the given upstream and downstream time intervals (see Tables 1–2). Note also that the range of observed upstream and downstream Alfvén Mach numbers $0.76 < M_A^* < 0.80$ compares very well with the approximate Walén slope of 0.73 in Figure 2a as predicted, e.g., by *Øieroset et al.* [2000].

[38] The second boundary near the earthward jet interval immediately following the enhanced tailward flow region also suggests the likely presence of a shock based on the increase in the H^+ entropy and the general balance of the upstream and downstream RH jump conditions (see Tables 1–2). However, the upstream energy flow (RH_3) and the tangential electric field (RH_6) are ~24% lower and ~48% larger, respectively, than the corresponding downstream RH quantities. The remaining jump conditions are all within 15% of being balanced. This suggests a larger degree of uncertainty in the shock jump conditions for this earthward flow event than for the tailward flow analysis. Moreover, the kinetic plasma pressure across the boundary stays rather constant. The magnetic field pressure, however, is ~27% lower downstream than on the upstream side and the magnetic field bends toward the estimated shock normal across this boundary. On the basis of these conditions alone,

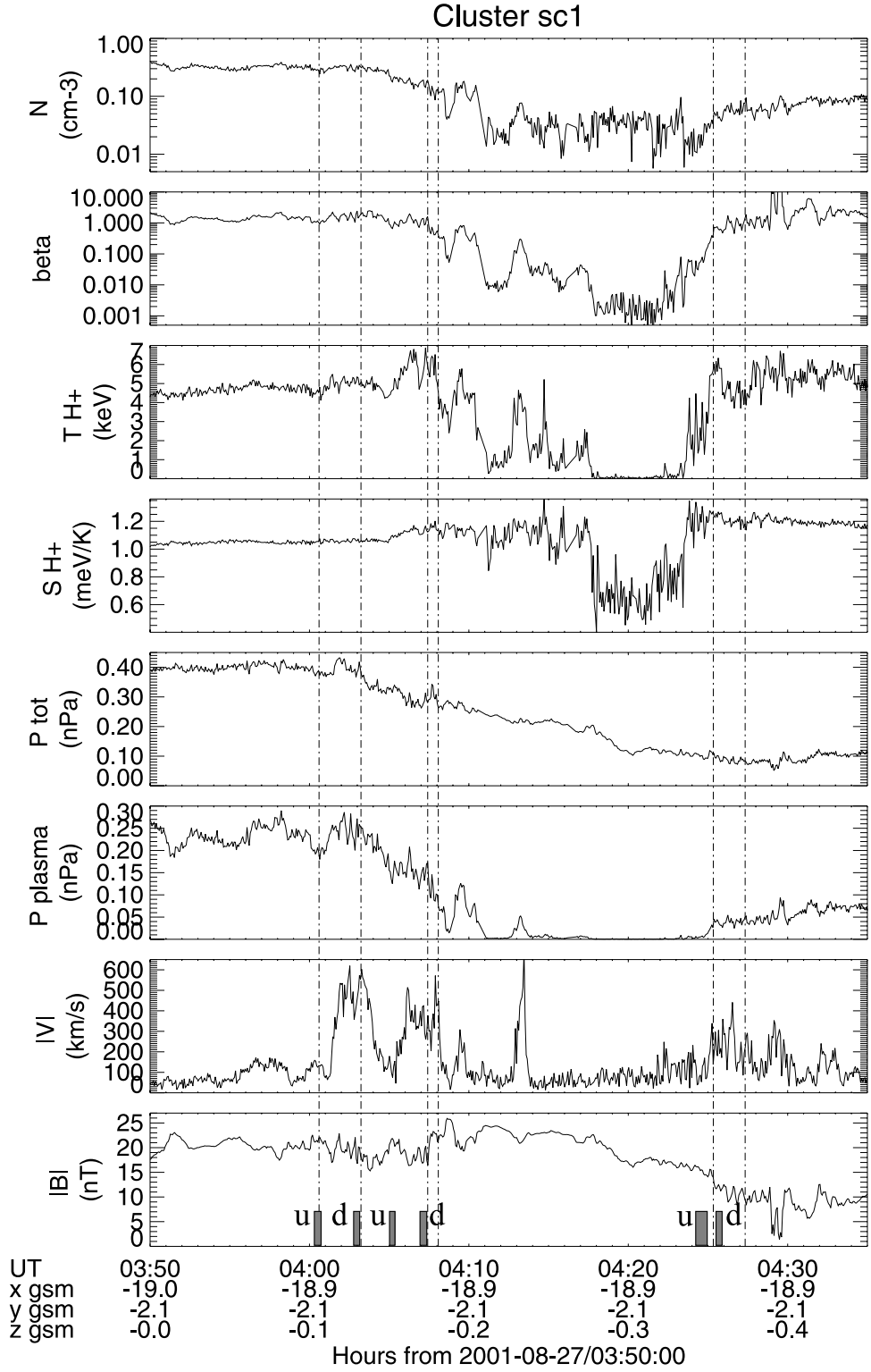

Figure 3. A number of plasma and magnetic field quantities relevant to the shock analysis are displayed. From the top, these are the total H^+ and O^+ plasma density N, the ion plasma β, the proton temperature, the total proton Sackur-Tetrode entropy, the total plasma and magnetic field pressure, the kinetic plasma pressure P_p, the observed plasma bulk speed, and the magnetic field magnitude. The selected three pairs of upstream and downstream time intervals are indicated by vertical bars in the last panel.

Table 1. Relative H^+ Entropy, Shock Normal (GSM), and Shock Velocity (GSM) for Three Shock Analysis Time Intervals on 27 August 2001 Using Cluster C1 Data[a]

Quantity	Shock Analysis I	Shock Analysis II	Shock Analysis III
Δt_u, UT	0400:19–0400:50	0405:03–0405:25	0424:15–0425:00
Δt_d, UT	0402:50–0403:10	0406:55–0407:25	0425:37–0425:55
ΔS, meV/K	$9.7 \cdot 10^{-3}$	$35.3 \cdot 10^{-3}$	$51.1 \cdot 10^{-3}$
n_x	0.489867	0.903475	0.278343
n_y	−0.865629	−0.416104	0.708950
n_z	−0.103523	0.102907	0.648008
V_x^{sh}, km/s	−349	−1189	114
V_y^{sh}, km/s	616	548	291
V_z^{sh}, km/s	74	−135	266
$\lvert \mathbf{V}_{sh} \rvert$, km/s[b]	−711	−1316	410

[a]The upstream and downstream time intervals are indicated between the vertical bars in Figure 3.
[b]The parallel or antiparallel direction of the shock speed along the shock normal is indicated by the sign.

it seems that the assumed shock has a slow-mode characteristic, although the kinetic pressure barely increases. We finally observe that the *Seon et al.* [1996] Mach number conditions are not fully satisfied, since $M_I^* > 1$ on the upstream side and $M_{SM}^* > 1$ on the downstream side of the shock. This suggests that the boundary is not slow-mode in character, if indeed it is a shock.

[39] For the last of the high-speed flow intervals, during what was likely to be the recovery phase of the substorm [*Baker et al.*, 2002], the H^+ temperature and entropy clearly increase from the upstream (lobe) to the downstream (plasma sheet) environment as expected at a shock (Table 1). Moreover, it is observed that the upstream normal momentum (RH_2) is only ∼17% higher than the downstream level. The tangential momentum across the assumed shock is clearly not balanced, however. It seems, furthermore, that the energy flow (RH_3) is ∼68% lower on the upstream side than on the downstream side of the boundary. It would be necessary to assume a rather large additional heat flux component in the upstream lobe-like region to balance the energy budget across this boundary if we assume it is a shock.

[40] We finally examine the slow-mode shock criteria for the last boundary and observe that (1) $P_p^d > P_p^u$, (2) $P_b^d < P_b^u$ by ∼60%, and (3) $\theta_B^u \sim 40°$ while $\theta_B^d \sim 10°$. These relations strongly indicate the presence of a slow-mode shock. Turning to the Mach number criteria, it is moreover found that (1) $M_I^* = 0.40$ on the lobe (upstream) side of the

Table 2. Rankine-Hugoniot and Slow-Mode Shock Analysis for Three Time Intervals on 27 August 2001 Using Cluster C1 Data

Quantity	0400:19 UT 0400:50 UT up	0402:50 UT 0403:10 UT down	0405:03 UT 0405:25 UT up	0406:55 UT 0407:25 UT down	0424:15 UT 0425:00 UT up	0425:37 UT 0425:55 UT down
ρ_f, 10^{-22} kg/m^3	6.08	6.87	4.66	3.57	0.89	1.35
V_x, km/s	−8.2	−466.0	−102.2	214.7	28.6	202.5
V_y, km/s	136.0	−40.4	−12.8	−243.9	−68.7	−9.0
V_z, km/s	−5.9	−35.5	−42.2	−98.3	−37.6	76.0
B_x, nT	17.6	7.4	11.1	17.5	11.5	4.9
B_y, nT	−12.1	−17.4	−18.1	−3.7	3.5	7.3
B_z, nT	1.4	−2.7	0.3	2.3	9.2	7.9
P_p, nPa	0.20	0.24	0.15	0.15	0.01	0.03
P_b, nPa	0.18	0.15	0.18	0.13	0.09	0.06
P_t, nPa	0.38	0.39	0.33	0.28	0.10	0.09
β	1.07	1.69	0.85	1.21	0.08	0.58
n_{H^+}, cm^{-3}	0.28	0.30	0.20	0.17	0.02	0.04
T_{H^+}, keV	4.5	5.1	4.8	5.7	2.4	5.6
S_{H^+}, meV/K	1.05	1.06	1.09	1.13	1.20	1.25
V_n, km/s	590	522	1225	1602	−475	−311
V_A, km/s	776	649	879	858	1554	928
θ_B, deg	27.9	11.4	34.2	14.8	40.0	9.9
V_I, km/s	686	636	728	829	1189	914
V_S, km/s	735	764	733	842	357	634
V_{SM}, km/s	550	612	524	733	270	617
M_A^*	0.76	0.80	1.39	1.87	0.31	0.33
M_I^*	0.86	0.82	1.68	1.93	0.40	0.34
M_S^*	0.80	0.68	1.67	1.90	1.33	0.49
M_{SM}^*	1.07	0.85	2.34	2.18	1.76	0.50
RH_1, 10^{-16} kg/m^{2}s	3.59 (100%)[a]	3.59	5.71 (100%)	5.71	0.42 (100%)	0.42
RH_2, nPa	0.59 (103%)	0.58	1.03 (86%)	1.20	0.12 (117%)	0.10
RH_3, 10^3 kg/s^3	290 (93%)	314	460 (76%)	608	−8 (32%)	−25
RH_4, nT	19.0 (100%)	19.0	17.6 (100%)	17.6	11.7 (100%)	11.7
RH_5, nPa	0.13 (110%)	0.12	0.13 (88%)	0.15	0.09 (353%)	0.03
RH_6, mV/m	5.0 (71%)	7.0	13.5 (148%)	9.1	5.2 (183%)	2.8

[a]The upstream RH parameter relative to the downstream parameter is indicated for each condition and shock interval.

boundary, (2) $M^*_{SM} = 1.76$ on the lobe (upstream) side, and (3) $M^*_{SM} = 0.50$ on the plasma sheet (downstream) side of the shock. Again, these Mach number criteria are fully consistent with a slow-mode shock [*Seon et al.*, 1996]. The range of upstream and downstream Alfvén Mach numbers are $0.31 < M^*_A < 0.33$, which compares well with the estimated Walén slope at 33% of the Alfvén velocity in Figure 2c, although the low correlation coefficient (cc = −0.54) reflects a considerable degree of scatter in the field-aligned velocity.

[41] In summary, these Cluster C1 data are consistent with slow-mode shocks in connection with the tailward flows (first interval in Figure 1) and most likely with the earthward flow region at the time of the plasma sheet recovery over Cluster (third interval in Figure 1). When comparing the GSM directions of the derived shock velocity $\mathbf{V}_{sh}$ (see Table 1) with the deHoffmann-Teller velocity $\mathbf{V}_{HT}$ in Figure 2 for these two flow regions, it is moreover clear that the shock frame and HT frame velocities point in approximately similar directions. The angle between $\mathbf{V}_{sh}$ and $\mathbf{V}_{HT}$ is ∼30° for the tailward case while ∼40° for the earthward case during the plasma sheet recovery. We conclude that the joint Walén analyses and shock analyses for these two events are consistent with the presence of nearby Petschek-type slow-mode shocks connected to a near-Earth neutral line across which the ions gained their acceleration.

4.2. Shock Normal Optimization

[42] The shock normal direction is expected to satisfy the magnetic coplanarity theorem as stated in equation (11) according to theoretical considerations for both fast-mode and slow-mode types of shocks [e.g., *Hau and Sonnerup*, 1989; *Burgess*, 1995]. However, any measurement is associated with a level of uncertainty that may result in a deviation from fully satisfied RH conditions. An optimization analysis is therefore performed for each of the three previously identified shock periods (see Table 1) in search of that unit normal direction $\hat{\mathbf{n}}_c = (n_x, n_y, n_z)$ for which the sum of the observed differences between the upstream and downstream sets of RH shock jump conditions are minimized.

[43] The applied method is based on the technique of *Seon et al.* [1996] that defines a function $\chi^2(\theta, \phi)$, where $\theta = \arccos(n_z)$ and $\phi = \arctan(n_y/n_x)$ are the spherical polar and azimuthal GSM coordinates of the normal unit sphere. Here, we define χ^2 as

$$\chi^2(\theta,\phi) \equiv \sum_{i=1}^{6} \left(\frac{X_i^u}{X_i^d} - 1\right)^2, i \neq 3, \qquad (15)$$

where X_i are the observed upstream and downstream MHD quantities from the RH shock jump conditions previously stated in equations (4)–(9). A larger degree of uncertainty is expected in the conservation of energy flow due to the exclusion of any additional heat flux component in equation (6). We therefore omit RH_3 in the definition of χ^2. A total number of $N_\theta \times N_\phi = 180 \times 360$ unit normals are considered, corresponding to an angular resolution of $\Delta\theta \times \Delta\phi = 1° \times 1°$ for the total set of normal vectors $\hat{\mathbf{n}}$ over the unit sphere. The χ^2 distribution is then searched for those $\hat{\mathbf{n}}$ directions that satisfy (1) $\chi^2 \leq \chi^2_{mc}$, where χ^2_{mc} corresponds to the unit normal $\hat{\mathbf{n}}_{mc}$ resulting from the magnetic coplanarity theorem (see Table 1), and (2) $(X_i^u/X_i^d - 1)^2 \leq \varepsilon^2$, where $\varepsilon = 0.15$ and $i \neq 3$.

[44] Figure 4 displays the optimization results for the first shock interval during the tailward flow interval near 0401 UT (see Table 1) with the polar and azimuthal dependent χ^2 distributions shown in Figures 4a–4b. The polar and azimuthal angles that correspond to χ^2_{mc} are marked by square symbols and dashed vertical lines in blue. The polar angle distribution of χ^2 is symmetric on either side of $\theta = 90°$ due to the two opposite $\pm\hat{\mathbf{n}}$ directions. The normal direction symmetry is also reflected in the azimuthal dependence of χ^2, which results in two pairs of local minima separated by $\Delta\phi = 180°$. The two unique minima at $\phi_a = 281°$ and $\phi_b = 302°$ are shown in Figure 4b with those unit directions corresponding to the 15% RH criteria and $\chi^2 \leq \chi^2_{mc}$ represented as blue dots. We further identify two subsets of normal directions around ϕ_a and ϕ_b from this data set that also satisfy the critical slow-mode shock requirements $M_f^* \leq 1.0$ and $M^*_{SM} > 1.0$ on the upstream side and $M^*_{SM} < 1.0$ on the downstream side. These subsets are displayed as red and green dots, respectively.

[45] An optimum unit normal $\hat{\mathbf{n}}_c$ is defined within the slow-mode subset related to the χ^2 minimum at ϕ_b and for that direction where the RH jump condition is also optimized for the normal magnetic field condition RH_3. The derived normal $\hat{\mathbf{n}}_c = (0.507213, -0.844145, -0.173648)$ is indicated by a red square and dashed red lines in Figures 4a–4b. This normal direction makes an angle of only ∼4.3° with $\hat{\mathbf{n}}_{mc}$ and suggests that the unit normal direction provided by the magnetic coplanarity theorem is a good approximation for the shock normal direction. The total χ^2 is also improved by an order of magnitude so that the corresponding upstream and downstream RH conditions for $\hat{\mathbf{n}}_c$ all agree within 10% as shown in Table 3.

[46] The range of slow-mode Mach numbers M^*_{SM} and Alfvén Mach numbers M^*_A for the three subsets are shown in Figures 4c–4d. The corresponding Mach numbers using the two normal directions $\hat{\mathbf{n}}_{mc}$ and $\hat{\mathbf{n}}_c$ are again depicted by the blue and red squares, respectively, with $M^*_{SM} = 1.23$ and $M^*_A = 0.87$ on the upstream side, while $M^*_{SM} = 0.98$ and $M^*_A = 0.92$ on the downstream side for $\hat{\mathbf{n}} = \hat{\mathbf{n}}_c$.

[47] An optimization analysis for the second shock period in connection with the earthward flows near 0407 UT fails to provide any evidence in favor of slow-mode shocks. However, an optimum shock normal direction is found within ∼26° of the $\hat{\mathbf{n}}_{mc}$ direction that improves the correspondence between the upstream and downstream RH conditions (see Table 3).

[48] The optimization results for the last shock analysis during the plasma sheet recovery phase are displayed in Figure 5. Only one unique χ^2 minimum is found during this period with the expected $\pm\hat{\mathbf{n}}$ symmetry. A search for those $\hat{\mathbf{n}}$ directions that satisfy (1) $\chi^2 \leq \chi^2_{mc}$ and (2) $(X_i^u/X_i^d - 1)^2 \leq \varepsilon^2$, where $\varepsilon = 0.15$ and $i \neq (3, 5)$ results in a total of 512 unique normal directions. A total of 462 normal directions from this subset or ∼90% also satisfy the critical slow-mode shock requirements and are displayed as green dots in Figures 5a–5b. The subset shown in red correspond to the oppositely directed shock normal directions.

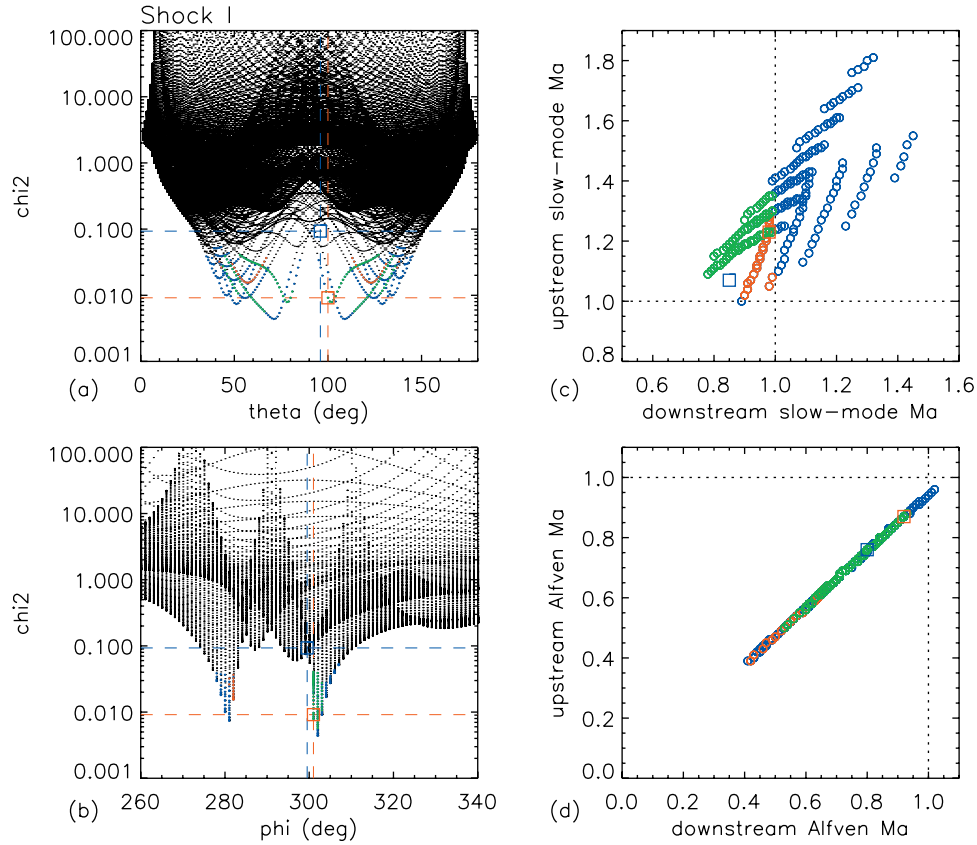

Figure 4. Shock normal optimization analysis for the plasma sheet shock during the tailward flow interval with (a) the polar θ-dependence of χ^2 and (b) the azimuthal ϕ-dependence displayed separately. The distributions for (c) the slow-mode Mach number and (d) the Alfvén Mach number are shown for the subsets of shock normal directions around the two ϕ-dependent χ^2 minima with improved RH conditions that also satisfy the critical slow-mode shock requirements (green and red). The χ^2 distributions and Mach numbers in blue correspond to normal directions where the Mach number requirements failed. Dashed blue lines and squares correspond to the normal direction from the coplanarity theorem, while the red squares and dashed lines indicate a normal direction within the "green" subset that yield an optimized normal magnetic field RH condition (see text for details).

[49] In omitting the conservation relations for both the energy flow (RH_3) and the tangential momentum (RH_5), it is possible to find a normal direction (red square in Figure 5) that results in smaller deviations (than otherwise obtained using $i \neq 3$) between the upstream and downstream normal magnetic fields while still improving the total χ^2 by nearly two orders of magnitude (see RH in Table 3). This optimum normal $\hat{\mathbf{n}}_c = (-0.262782, -0.128167, 0.956305)$ makes an angle of $\sim 63^\circ$ with the estimated $\hat{\mathbf{n}}_{mc}$ from the magnetic coplanarity theorem. The large normal deviation may be related to the fact that the selected upstream and downstream intervals are typical of the low-β lobe and the high-β plasma sheet regions (see Figure 3) that always will appear as a quantitative slow-mode transition. However, the identification of the boundary as a slow-mode shock is still consistent with the critical Mach number requirements for the optimized shock normal (red square in Figures 5c–5d), since $M_I^* = 0.29$ and $M_{SM}^* = 1.31$ on the upstream side and $M_{SM}^* = 0.43$ on the downstream side of the boundary.

[50] The lower Alfvén Mach numbers obtained on either side of the boundary using $\hat{\mathbf{n}}_c$ (red square in Figure 5d) suggest that a relatively lower regression slope should be expected in the HT frame of reference when the Walén analysis is applied to these high-speed flows near the plasma sheet boundary layer. An opposite tendency toward higher M_A^* resulted from the optimized normal analysis when it was applied to the tailward flows within the plasma sheet proper (see Figure 4d). Whether this is a coincidence or not is impossible to say based on this single event study. It is concluded, however, that the presence of slow-mode shocks are confirmed in connection with the high-speed tailward flow region in the plasma sheet and the earthward flow region during the plasma sheet recovery on the basis of these shock normal optimization analyses.

5. Discussion

[51] The mean location of the near-Earth neutral line is statistically expected near $x_{GSM} = -25\ R_E$ based on Geotail observations [*Nagai et al.*, 1998]. The Cluster measurements presented here strongly suggest that a reconnection site initially formed in the plasma sheet earthward of Cluster which was located north of the neutral sheet ($B_x > 0$) at $x_{GSM} = -19\ R_E$.

Table 3. Optimized Shock Normal Directions and the Corresponding Mach Numbers Based on the Observed Rankine-Hugoniot Conditions for Shocks I, II, and III (See Definitions in Table 1)

Quantity	Shock I	Shock II	Shock III
n_x	0.507213	0.871268	−0.262782
n_y	−0.844145	−0.352015	−0.128167
n_z	−0.173648	−0.342020	0.956305
$\theta_{B,u}$, deg	28.2	41.5	69.6
$\theta_{B,d}$, deg	12.2	30.0	63.3
$M^*_{I,u}$	0.98	1.86	0.29
$M^*_{SM,u}$	1.23	2.66	1.31
$M^*_{SM,d}$	0.98	2.66	0.43
$M^*_{A,u}$	0.87	1.39	0.10
$M^*_{A,d}$	0.92	1.87	0.11
RH^u_1, 10^{-16} kg/m^{2}s	4.0927 (100.0%)[a]	5.7137 (100.0%)	0.1412 (100.0%)
RH^d_1, 10^{-16} kg/m^{2}s	4.0927	5.7137	0.1412
RH^u_2, nPa	0.6555 (103.5%)	1.0302 (85.9%)	0.1012 (112.7%)
RH^d_2, nPa	0.6331	1.1988	0.0898
RH^u_3, 10^3 kg/s^3	331.22 (92.5%)	460.40 (75.7%)	−2.70 (31.7%)
RH^d_3, 10^3 kg/s^3	357.97	608.18	−8.52
RH^u_4, nT	18.9117 (100.0%)	15.9359 (101.0%)	5.3088 (100.0%)
RH^d_4, nT	18.9103	15.7712	5.3093
RH^u_5, nPa	0.1358 (98.0%)	0.1767 (112.6%)	0.0599 (128.7%)
RH^d_5, nPa	0.1385	0.1570	0.0465
RH^u_6, mV/m	6.0579 (91.3%)	17.0149 (114.3%)	2.2725 (112.4%)
RH^d_6, mV/m	6.6328	14.8868	2.0224

[a]The upstream RH parameter relative to the downstream parameter is indicated for each condition and shock interval.

[52] The neutral line region generated an interval of tailward plasma flows that satisfied the Walén test with the expected positive slope [*Øieroset et al.*, 2000]. Furthermore, the sub-Alfvénic field-aligned velocity in the HT frame at 73% of the Alfvén velocity compared well with the upstream and downstream Alfvén Mach number in a confirmed slow-mode shock frame (see Tables 2–3). The connection of a Petschek-type slow-mode shock with a near-Earth neutral line is also apparent from the general agreement between the direction of the shock velocity $\mathbf{V}_{sh}$ = (−349, 616, 74) km/s (see Table 1) and that of the deHoffmann-Teller frame velocity $\mathbf{V}_{HT}$ = (−595, 362, −23) km/s (see Figure 2). The separation angle between these vectors is ∼30°. A clear deflection of the magnetic field was further observed in the negative B_y direction (peak $B_y \sim -20$ nT) which is consistent with the direction of the predicted Hall magnetic field in this region north of the neutral sheet and tailward of the neutral line [see, e.g., *Sonnerup*, 1979; *Runov et al.*, 2003].

[53] The magnetic field rotation from positive B_x to negative B_y and a negative B_z component during the tailward flow interval is also consistent with the presence of a plasmoid taking off downtail with a $B_y < 0$ core field direction. The sudden release in the total plasma and magnetic field pressure (see fourth panel from the bottom of Figure 3) from ∼0.43 nPa at the beginning of the tailward flow region to ∼0.25 nPa at the approximate reversal to earthward flows lends further support to the downtail release of a plasmoid. Further evidence of plasmoid formation is also given by the observation of a smaller-scale plasmoid-type magnetic flux rope [*Slavin et al.*, 2003a] that was detected during the leading edge of the tailward flow interval. Small-scale plasma sheet flux ropes are often reported near the leading edges of earthward and tailward high-speed flows in the near-Earth magnetotail [*Slavin et al.*, 2003a, 2003b] and are regarded as strong evidence in favor of multiple X-line reconnection [e.g., *Deng et al.*, 2004].

[54] The subsequent earthward plasma flows suggest that the neutral line either propagated downtail over the spacecraft or that it reformed on the tailward side of Cluster. The observed plasma velocity and the magnetic field data neither satisfied the Walén analysis (see Figure 2b) for this earthward flow interval, nor could we confirm the presence of a slow-mode shock (Tables 1–3). The observed negative B_y component of the magnetic field during this interval neither satisfies that of the expected positive Hall B_y field. The failure of these quantitative tests may be due to instabilities caused by the near-Earth magnetic field pressure gradient [e.g., *Shiokawa et al.*, 1998] and their effects on the assumption of quasi-steady shocks.

[55] The earthward flow region in connection with the probable plasma sheet recovery at ∼0426 UT (see Figure 1) clearly suggests the passage of a slow-mode shock based on the critical slow-mode shock requirements [*Seon et al.*, 1996] that likely resulted in the expected negative Walén slope in Figure 2c. The magnetic field (see Figure 1) further displayed a change in the positive B_y direction (peak $B_y \sim$ 8 nT) as would be expected for a Hall-type magnetic field deflection earthward of a near-Earth X-line. Moreover, the field-aligned velocity estimate in the HT frame corresponds to ∼33% of the Alfvén velocity which compares well with the sub-Alfvénic range of upstream M^*_A = 0.31 and downstream M^*_A = 0.33 (see Table 2). Although the range of M^*_A is reduced to $M^*_A \sim 0.10$ when applying the optimized normal direction (see Figure 5), it should be noted that there is some uncertainty related to the Walén slope as well due to the rather poor correlation coefficient of only cc = −0.54.

[56] The considerable degree of variance in the measured velocity in the HT frame (see Figure 2c) may reflect the influence of the obstacle posed by the near-Earth magnetic field [*Shiokawa et al.*, 1998; *Priest and Forbes*, 2000] on the assumption of time independence when

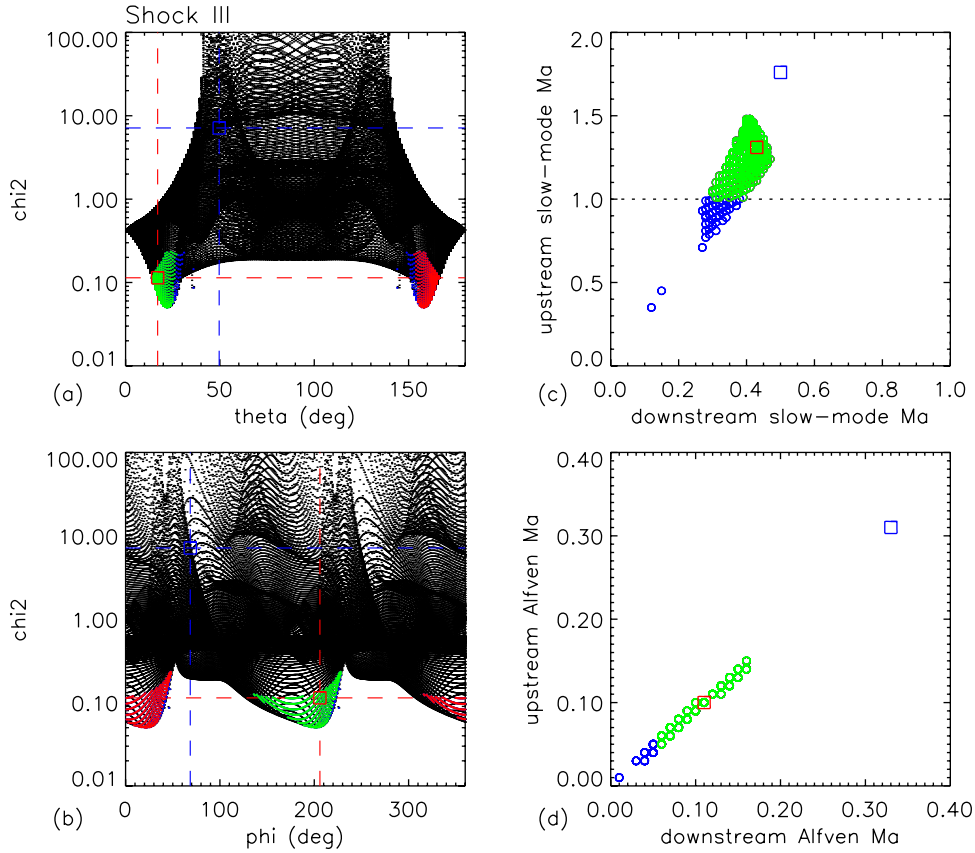

Figure 5. Shock normal optimization analysis for the shock boundary detected during earthward plasma flow between the upstream magnetotail lobe and the downstream plasma sheet. Same format as Figure 4. One unique ϕ-dependent χ^2 minimum is observed at $\phi = 201°$. All normal directions with improved RH conditions that correspond to satisfied slow-mode shock requirements around $\phi = 201°$ ($\phi = 21°$) are shown in green (red). The χ^2 distribution and Mach numbers in blue correspond to normal directions where the Mach number requirements failed. A red square indicate a normal direction that yield an optimized normal magnetic field RH condition within the "green" subset.

applying the Walén test. The observed large deviation between the upstream and downstream (dominant) Rankine-Hugoniot energy flow condition also weakens the quasi-steady slow-mode shock argument for this earthward flow interval. Recall, however, that no additional heat flux component was included in the RH shock jump condition (see equation (6)).

[57] As illustrated in an electromagnetic hybrid code simulation of slow-mode shocks in low β plasmas [e.g., *Omidi and Winske*, 1989], a substantial fraction of backstreaming ions may leak into the upstream region from the downstream ion population as was also confirmed by in situ measurements from the Geotail spacecraft in the distant magnetotail [*Saito et al.*, 1996]. Such fluxes may account for some of the energy budget offset in the low ion β environment (see Tables 2–3) that the Cluster spacecraft encountered between the lobe region and the plasma sheet during the recovery phase.

[58] There are several reports on successful shock analyses performed between the interface of the magnetotail lobe and the plasma sheet [e.g., *Seon et al.*, 1996] where these regions are given as the upstream and downstream regions, respectively. However, for our first slow shock boundary near ~0401 UT, reconnection had just been initiated in the plasma sheet and had not yet proceeded to lobe field lines [*Baker et al.*, 2002]. The RH jump conditions were satisfied for the upstream and downstream intervals for this event, implying the presence of slow shocks connected to a neutral line in the plasma sheet.

6. Summary and Conclusions

[59] Using Cluster data from the CIS and FGM instruments, we have shown that an interval of enhanced tailward flows in the very near-Earth plasma sheet at $x \sim -19\ R_E$ is in quantitative agreement with magnetic reconnection in connection with slow-mode shocks. A single substorm also occurred during this 27 August 2001 event and was described in detail by *Baker et al.* [2002].

[60] The evidence consists of sub-Alfvénic field-aligned velocities in the deHoffmann-Teller frame of reference as based on the Walén test together with the following fully satisfied slow-mode shock criteria between the upstream and the downstream sides of the shock: (1) the ion entropy increased downstream, (2) the plasma pressure

P_p increased across the shock, (3) the magnetic pressure P_b decreased across the shock, (4) the propagation angle θ_B of the direction of the wave decreased downstream (i.e., the magnetic field bent toward the shock normal direction), (5) the upstream intermediate Alfvén Mach number $M_I^* \leq 1.0$, (6) the upstream slow-mode magnetosonic Mach number $M_{SM}^* > 1.0$, and (7) the downstream slow-mode magnetosonic Mach number $M_{SM}^* < 1.0$. The positive Walén slope is consistent with accelerated flows across a slow shock on the tailward side of a neutral line in the Northern Hemisphere. The upstream and downstream Alfvén Mach numbers also compared well with the sub-Alfvénic Walén slope.

[61] The fast earthward flows detected immediately after the tailward flows, however, did not satisfy these slow-mode shock requirements, nor did they satisfy the Walén test. Our single event study suggests that the shocks and the accelerated plasma on the earthward side of the neutral line were indeed more directly affected by the obstacle of the stronger near-Earth magnetic field [e.g., *Priest and Forbes*, 2000, and references therein].

[62] The earthward flow region observed during the plasma sheet recovery satisfied the basic slow-mode criteria listed above, but the Rankine-Hugoniot shock jump relation for the energy flow was not consistent with that of a shock unless a very large heat flux component would be added to the upstream (lobe) side of the assumed shock. Such a heat flux may originate in low β plasmas from the leakage of hotter backstreaming ions from the downstream side of the shock [e.g., *Omidi and Winske*, 1989; *Saito et al.*, 1996]. Moreover, the Walén test suggests a regression slope of the correct sign (negative) in this region north of the neutral sheet and on the earthward side of the assumed near-Earth neutral line. The derived Walén slope is also consistent with the range of upstream and downstream Alfvén Mach numbers in the frame of the slow-mode shock.

[63] **Acknowledgments.** We thank both reviewers for their comments. This work is supported by NASA grant NAG5-10108 through Boston University (GC 174055) and by NASA grant NAG5-12941 at the University of California, Berkeley.

[64] Arthur Richmond thanks Tsugunobu Nagai and James A. Slavin for their assistance in evaluating this paper.

References

Angelopoulos, V., W. Baumjohann, C. F. Kennel, F. V. Coroniti, M. G. Kivelson, R. Pellat, R. J. Walker, H. Lühr, and G. Paschmann (1992), Bursty bulk flows in the inner central plasma sheet, *J. Geophys. Res.*, *97*, 4027.

Baker, D. N., T. I. Pulkkinen, V. Angelopoulos, W. Baumjohann, and R. L. McPherron (1996), Neutral line model of substorms: Past results and present view, *J. Geophys. Res.*, *101*, 12,975.

Baker, D. N., et al. (2002), Timing of magnetic reconnection initiation during a global magnetospheric substorm onset, *Geophys. Res. Lett.*, *29*(24), 2190, doi:10.1029/2002GL015539.

Balogh, A., et al. (2001), The Cluster magnetic field investigation: Overview of in-flight performance and initial results, *Ann. Geophys.*, *19*, 1207.

Baumjohann, W., G. Paschmann, and H. Lühr (1990), Characteristics of high speed ion flows in the plasma sheet, *J. Geophys. Res.*, *95*, 3801.

Burgess, D. (1995), Collisionless shocks, in *Introduction to Space Physics*, edited by M. G. Kivelson and C. T. Russell, pp. 129–163, Cambridge Univ. Press, New York.

deHoffmann, F., and E. Teller (1950), Magnetohydrodynamic shocks, *Phys. Rev.*, *80*, 692.

Deng, X. H., H. Matsumoto, H. Kojima, T. Mukai, R. R. Anderson, W. Baumjohann, and R. Nakamura (2004), Geotail encounter with reconnection diffusion region in the Earth's magnetotail: Evidence of multiple X lines collisionless reconnection?, *J. Geophys. Res.*, *109*, A05206, doi:10.1029/2003JA010031.

Dungey, J. W. (1961), Interplanetary magnetic field and the auroral zones, *Phys. Rev. Lett.*, *6*, 47.

Escoubet, C. P., M. Fehringer, and M. Goldstein (2001), The Cluster mission, *Ann. Geophys.*, *19*, 1197.

Feldman, W. C., et al. (1984), Evidence for slow-mode shocks in the deep geomagnetic tail, *Geophys. Res. Lett.*, *11*, 599.

Feldman, W. C., R. L. Tokar, J. Birn, E. W. Hones Jr., S. J. Bame, and C. T. Russell (1987), Structure of a slow mode shock observed in the plasma sheet boundary layer, *J. Geophys. Res.*, *92*, 83.

Hau, L.-N., and B. U. Ö. Sonnerup (1989), On the structure of resistive MHD intermediate shocks, *J. Geophys. Res.*, *94*, 6539.

Hones, E. W., Jr., T. A. Fritz, J. Birn, J. Cooney, and S. J. Bame (1986), Detailed observations of the plasma sheet during a substorm on April 24, 1979, *J. Geophys. Res.*, *91*, 6845.

Khrabrov, A. V., and B. U. Ö. Sonnerup (1998), DeHoffmann-Teller analysis, in *Analysis Methods for Multi-Spacecraft Data*, edited by G. Paschmann and P. W. Daly, *ISSI Sci. Rep., SR-001*, pp. 221–248, Eur. Space Agency, Paris.

Nagai, T., M. Fujimoto, Y. Saito, S. Machida, T. Terasawa, R. Nakamura, T. Yamamoto, T. Mukai, A. Nishida, and S. Kokubun (1998), Structure and dynamics of magnetic reconnection for substorm onsets with Geotail observations, *J. Geophys. Res.*, *103*, 4419.

Nagai, T., I. Shinohara, M. Fujimoto, M. Hoshino, Y. Saito, S. Machida, and T. Mukai (2001), Geotail observations of the Hall current system: Evidence of magnetic reconnection in the magnetotail, *J. Geophys. Res.*, *106*, 25,929.

Nagai, T., I. Shinohara, M. Fujimoto, S. Machida, R. Nakamura, Y. Saito, and T. Mukai (2003), Structure of the Hall current system in the vicinity of the magnetic reconnection site, *J. Geophys. Res.*, *108*(A10), 1357, doi:10.1029/2003JA009900.

Øieroset, M., T. D. Phan, R. P. Lin, and B. U. Ö. Sonnerup (2000), Walén and variance analyses of high-speed flows observed by Wind in the midtail plasma sheet: Evidence for reconnection, *J. Geophys. Res.*, *105*, 25,247.

Omidi, N., and D. Winske (1989), Structure of slow magnetosonic shocks in low beta plasmas, *Geophys. Res. Lett.*, *16*, 907.

Petschek, H. E. (1964), Magnetic field annihilation, in *AAS-NASA Symposium on Solar Flares*, *NASA Spec. Publ. SP-50*, p. 425, NASA, Washington, D. C.

Phan, T. D., B. U. Ö. Sonnerup, and R. P. Lin (2001), Fluid and kinetics signatures of reconnection at the dawn tail magnetopause: Wind observations, *J. Geophys. Res.*, *106*, 25,489.

Priest, E., and T. Forbes (2000), *Magnetic Reconnection: MHD Theory and Applications*, Cambridge Univ. Press, New York.

Rème, H., et al. (2001), First multispacecraft ion measurements in and near the Earth's magnetosphere with the identical Cluster ion spectrometry (CIS) experiment, *Ann. Geophys.*, *19*, 1303.

Runov, A., et al. (2003), Current sheet structure near magnetic X-line observed by Cluster, *Geophys. Res. Lett.*, *30*(11), 1579, doi:10.1029/2002GL016730.

Saito, Y., T. Mukai, T. Terasawa, A. Nishida, S. Machida, M. Hirahara, K. Maezawa, S. Kokubun, and T. Yamamoto (1995), Slow-mode shocks in the magnetotail, *J. Geophys. Res.*, *100*, 23,567.

Saito, Y., T. Mukai, T. Terasawa, A. Nishida, S. Machida, S. Kokubun, and T. Yamamoto (1996), Foreshock structure of the slow-mode shocks in the Earth's magnetotail, *J. Geophys. Res.*, *101*, 13,267.

Seon, J., L. A. Frank, W. R. Paterson, J. D. Scudder, F. V. Coroniti, S. Kokubun, and T. Yamamoto (1996), Observations of slow-mode shocks in Earth's distant magnetotail with the Geotail spacecraft, *J. Geophys. Res.*, *101*, 27,383.

Shiokawa, K., et al. (1998), High-speed ion flow, substorm current wedge, and multiple Pi 2 pulsations, *J. Geophys. Res.*, *103*, 4491.

Slavin, J. A., R. P. Lepping, J. Gjerloev, D. H. Fairfield, M. Hesse, C. J. Owen, M. B. Moldwin, T. Nagai, A. Ieda, and T. Mukai (2003a), Geotail observations of magnetic flux ropes in the plasma sheet, *J. Geophys. Res.*, *108*(A1), 1015, doi:10.1029/2002JA009557.

Slavin, J. A., et al. (2003b), Cluster electric current density measurements within a magnetic flux rope in the plasma sheet, *Geophys. Res. Lett.*, *30*(7), 1362, doi:10.1029/2002GL016411.

Smith, E. J., J. A. Slavin, B. T. Tsurutani, W. C. Feldman, and S. J. Bame (1984), Slow mode shocks in the Earth's magnetotail: ISEE-3, *Geophys. Res. Lett.*, *11*, 1054.

Sonnerup, B. U. Ö. (1979), Magnetic field reconnection, in *Solar System Plasma Physics*, vol. 3, edited by L. T. Lanzerotti, C. F. Kennel, and E. N. Parker, pp. 45–108, North-Holland, New York.

Sonnerup, B. U. Ö., I. Papamastorakis, G. Paschmann, and H. Lühr (1987), Magnetopause properties from AMPTE/IRM observations of the convection electric field: Method development, *J. Geophys. Res.*, *92*, 12,137.

Walén, C. (1944), On the theory of sunspots, *Ark. Mat. Astron. Fys.*, *30A*(15), 1.

D. N. Baker, R. E. Ergun, and S. Eriksson, Laboratory for Atmospheric and Space Physics, University of Colorado, 1234 Innovation Drive, Boulder, CO 80303, USA. (eriksson@lasp.colorado.edu)

A. Balogh, The Blackett Laboratory, Imperial College, Prince Consort Road, London, SW7 2BZ, UK.

M. W. Dunlop, Space Sciences Division, Rutherford Appleton Laboratory, Chilton, Didcot, Oxfordshire, OX11 0QX, UK.

C. Mouikis, Space Science Center, University of New Hampshire, Durham, NH 03824, USA.

M. Øieroset, Space Sciences Laboratory, University of California, Centennial Drive at Grizzly Peak Blvd., Berkeley, CA 94720-7450, USA.

H. Rème, Centre d'Etude Spatiale des Rayonnements, 9 Ave Colonel Roche, Cedex, Toulouse, 31029, France.

A. Vaivads, Swedish Institute of Space Physics, Box 537, SE-75121, Uppsala, Sweden.